Back-Illuminated Single-Photon Avalanche Diodes and Avalanche-Mode Light Emitting Diodes Based on Standard CMOS Technology

Doyoon Eom

The Graduate School

Yonsei University

Department of Electrical and Electronic Engineering

Back-Illuminated Single-Photon Avalanche Diodes and Avalanche-Mode Light Emitting Diodes Based on Standard CMOS Technology

A Master's Thesis

Submitted to the Department of Electrical and Electronic Engineering

and the Graduate School of Yonsei University

Doyoon Eom

December 2022

This certifies that the master's thesis of Doyoon Eom is approved.

Thesis Supervisor: Prof. Woo-Young Choi

Thesis Co-Supervisor: Ph.D. Myung-Jae Lee

Prof. Youngcheol Chae

The Graduate School

Yonsei University

December 2022

Table of Contents

Table of Contents i

List of Figures iv

List of Tables vi

Abstract vii

1. Introduction 1

1.1. SPAD 1

1.2. SPAD in CMOS Technology 2

1.3. Back-Illuminated SPAD (BI SPAD) 3

1.4. Avalanche-Mode LED (AMLED) 5

1.5. Motivation 7

1.6. Outline 9

2. Principle and Characteristics 10

2.1. Operation of SPAD 10

2.2. SPAD Parameters 11

2.2.1. I-V Characteristics 11

2.2.2. DCR 12

2.2.3. LET 13

2.2.4. PDP 14

2.2.5. Timing Jitter 16

2.3. Operation of AMLED 17

3. SPAD 19

3.1. Structures 19

3.2. Experiment Results 20

4. AMLED 35

4.1. Structures 35

4.2. Experiment Results 36

5. Conclusion 39

Reference 41

Abstract in Korean 45

List of Figures

Fig. 1-1. Geiger Mode APD (SPAD) 1

Fig. 1-2. Cross-section of a FI SPAD 4

Fig. 1-3. Cross-section of a BI SPAD 4

Fig. 1-4. Electroluminescence of Si LED 6

Fig. 1-5. Conventional configuration of pixel 7

Fig. 1-6. Best configuration of pixel: 3D stacking 8

Fig. 1-7. Alternative configuration of pixel 8

Fig. 2-1. Operation principle of SPAD 10

Fig. 2-2. I-V characteristics of a SPAD 12

Fig. 2-3. Dark count rate (DCR) of a SPAD 13

Fig. 2-4. Light emission test (LET) of a SPAD: (a) uniform shape, (b) ring shape 14

Fig. 2-5. Photon detection probability (PDP) of a SPAD 15

Fig. 2-6. Timing jitter of a SPAD 16

Fig. 2-7. Operation principle of a LED: (a) Forward-mode, (b) Momentum spread of carriers, (c) Avalanche-mode 18

Fig. 3-1. Cross-section of (a) FI SPAD, (b) BI SPAD 19

Fig. 3-2. I-V characteristics of the BI SPAD 20

Fig. 3-3. DCR comparison of FI SPAD and BI SPAD 21

Fig. 3-4. The relationship between DCR and temperature: (a) FI SPAD, (b) BI SPAD 23

Fig. 3-5. The Arrhenius plot at high temperature: (a) FI SPAD, (b) BI SPAD 23

Fig. 3-6. The Arrhenius plot at low temperature: (a) FI SPAD, (b) BI SPAD 24

Fig. 3-7. LET results under the same illuminated conditions: (a) FI SPAD at V_E = 3V, (b) BI SPAD at V_E = 3V 25

Fig. 3-8. PDP of the BI SPAD at V_E = 1V, 2V, 3V 26

Fig. 3-9. PDP comparison between FI SPAD and BI SPAD at V_E = 3V 27

Fig. 3-10. Depth information of the BI SPAD 28

Fig. 3-11. Absorption length according to the wavelength in Si 29

Fig. 3-12. Doping profile of the BI SPAD with TCAD simulation 30

Fig. 3-13. Reflection by metal reflector depending on the wavelength with TCAD simulation ········ 31

Fig. 3-14. Timing jitter results at 940 nm: (a) FI SPAD, (b) BI SPAD ········ 33

Fig. 4-1. Structures of AMLED: (a) Deep structure, (b) Shallow structure ········ 35

Fig. 4-2. LET results of deep junction structure: (a) before the breakdown voltage, (b) after the breakdown voltage (V_E = 3V) ········ 37

Fig. 4-3. LET results of shallow junction structure: (a) before the breakdown voltage, (b) after the breakdown voltage (V_E = 3V) ········ 37

Fig. 4-4. EL result of deep junction and shallow junction ········ 38

List of Table

Table. 1. Summary and comparison of the state-of-the-art BI SPADs ········ 34

Abstract

Back-Illuminated Single-Photon Avalanche Diodes and Avalanche-Mode Light Emitting Diodes Based on Standard CMOS Technology

Doyoon Eom

Dept. of Electrical and Electronic Engineering

The Graduate School, Yonsei University, Seoul, Korea

The single-photon avalanche diode (SPAD) manufactured in the complementary metal-oxide-semiconductor (CMOS) technology are highly required in several applications such as imaging and ranging, quantum communications and networks, biology, chemistry, astronomy, etc. Especially for emerging applications like light

detection and ranging (LiDAR) for autonomous vehicles and 3D scanners.

Conventionally, front-illuminated (FI) SPADs have been used, but they have limitations in having low efficiency in long wavelengths because the absorbed depth is shallow. Therefore, in this thesis, a back-illuminated (BI) SPAD structure in which the long-wavelength efficiency is optimized is proposed. The BI SPAD has a P-well/Deep N-well junction and was fabricated using DB Hitek 110 nm BI CIS technology. As a result, it was confirmed that the proposed BI SPAD had a three times higher 940 nm PDP than that of the existing FI SPAD, without a significant increase in noise characteristics. And in this thesis, the operation of the Si LED array manufactured by the standard CMOS technology in the visible range was confirmed by acting in the avalanche region. The possibility of an actual LED application was also confirmed through the measurement of LET and EL of two structures with different junction depths.

Keywords: single-photon avalanche diode (SPAD), front-illuminated (FI), back-illuminated (BI), photodetector, photodiode, light detection and ranging (LiDAR),

dark count rate (DCR), photon detection probability (PDP), light emission test (LET), timing jitter, light emitting diode (LED), avalanche-mode

1. Introduction

1.1. SPAD

A single-photon avalanche photodiode (SPAD) is a kind of avalanche photodiode (APD) just operating in different reverse bias voltage. A typical APD operates at near breakdown voltage. But the SPAD is operated above breakdown voltage, so has extremely high gain. This is called Geiger mode (Fig. 1-1) [1]. The SPAD is highly required in several applications such as light detection and ranging (LiDAR) for autonomous vehicles and 3D imagers [2], [3].

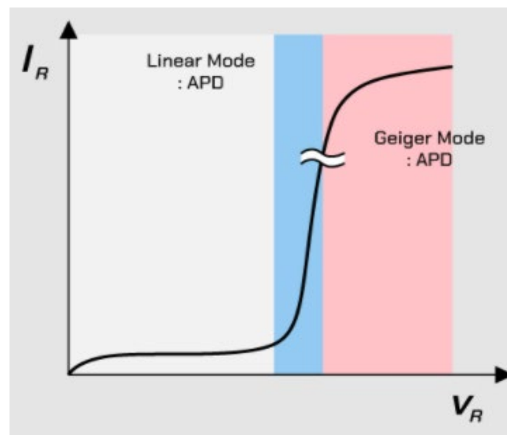

Fig. 1-1. Geiger Mode APD (SPAD)

1.2. SPAD in CMOS Technology

Previously, it was fabricated using a custom process to optimize SPAD [4], [5]. However, for various reasons, SPAD is gradually being produced using the CMOS technology [6], [7]. In CMOS technology, there are several advantages in terms of low manufacture cost, ability to enable monolithic integration with circuitry and large monolithic arrays [8]. In addition, the efficiency has been improved by using CMOS image sensor (CIS) technology with relatively low doping, rather than logic CMOS technology with high doping concentration [9], [10]. This is because a wider depletion region can be formed through lower doping concentration.

1.3. Back-Illuminated SPAD (BI SPAD)

Conventional CMOS-compatible SPADs are a front-illuminated (FI) type as shown in Fig.1-2 [11], but the FI structure has inherent limitations. The metals over the SPAD reduce the effective active area. In addition, FI SPADs have a low detection efficiency in the near-infrared (NIR) wavelengths because the PN junctions formed in CMOS technology are more shallow than the absorption length of NIR. To overcome these limitations, back-illuminated (BI) SPADs are good candidates. In BI SPADs, an example is shown in Fig. 1-3, the placement of the metal is opposite to the side where the light is incident, and therefore, they can decrease an injection loss. In addition, the detection efficiency in NIR increases as the junction becomes deeper and the metal over the device works as a light reflector [12].

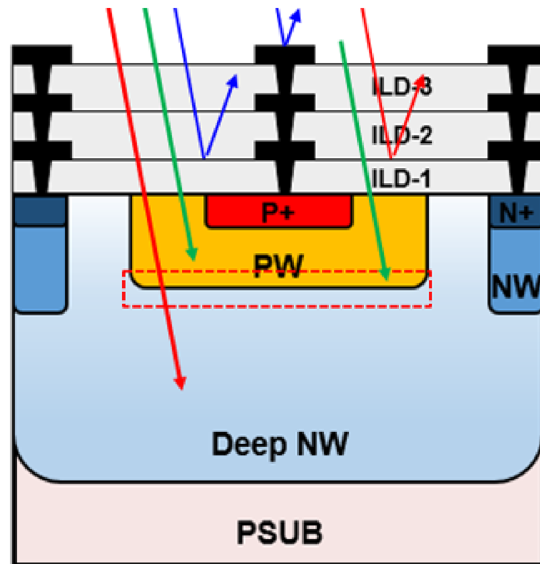

Fig. 1-2. Cross-section of a FI SPAD

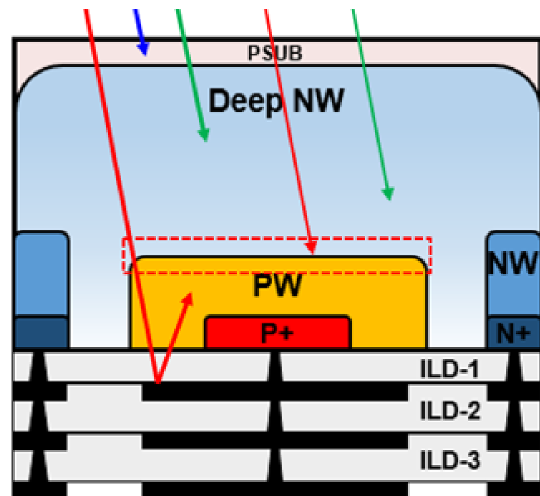

Fig. 1-3. Cross-section of a BI SPAD

1.4. Avalanche-Mode LED (AMLED)

A light-emitting diodes (LEDs) is widely used in many applications like displays, general illuminations, and communications. Because LEDs must emit light in the visible region for many applications, LEDs are typically fabricated based on III-V materials. However, III-V LEDs have a complicated process and high manufacturing cost. Therefore, Si LEDs through CMOS technology can be used instead, not only cost aspects but monolithic integration with circuits will be possible. In general, Si LEDs in forward-mode (FM) emit light in the 900-1200 nm wavelength [13], [14], so they cannot replace III-V LEDs. However, in avalanche region operation, a Si LED can substitute the conventional LEDs because it emits light in the visible region (Fig. 1-4). These LEDs are called avalanche-mode LEDs (AMLEDs) [15-18].

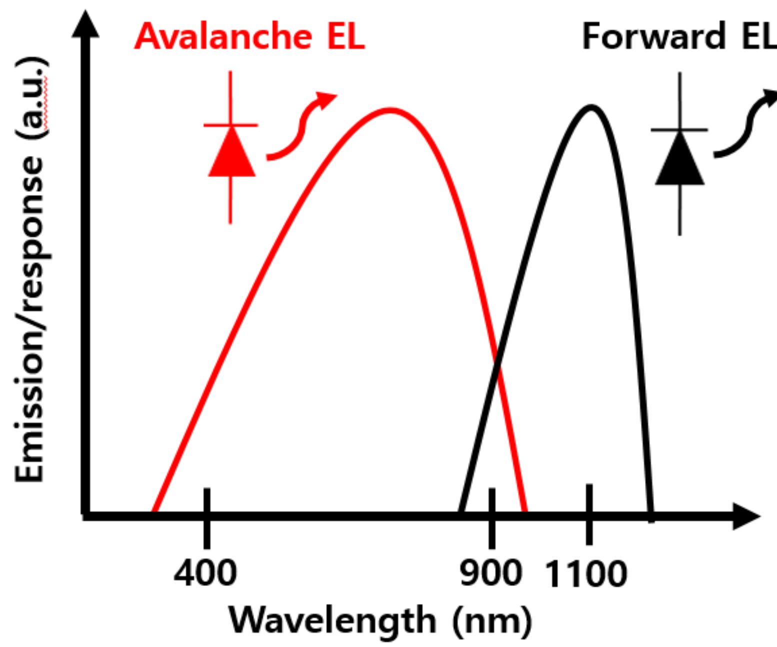

Fig. 1-4. Electroluminescence of Si LED

1.5. Motivation

When manufacturing LiDAR using SPAD, it is mainly composed as shown in Fig. 1-5. However, for high efficiency, it is needed to improve near-infrared (NIR) detection efficiency. Best approach is to stack SPAD in a 3D structure by inverting it like Fig. 1-6 [19], [20]. But because of complications of the process and high cost, it is still only being carried out by some leading companies. In this case, the placement in Fig. 1-7 could be a good alternative. By using BI SPAD instead of FI SPAD, NIR detection efficiency can be improved with no additional cost.

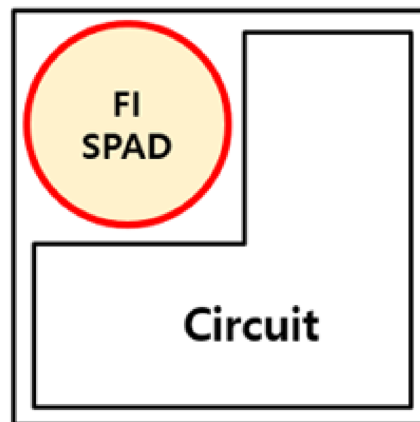

Fig. 1-5. Conventional configuration of pixel

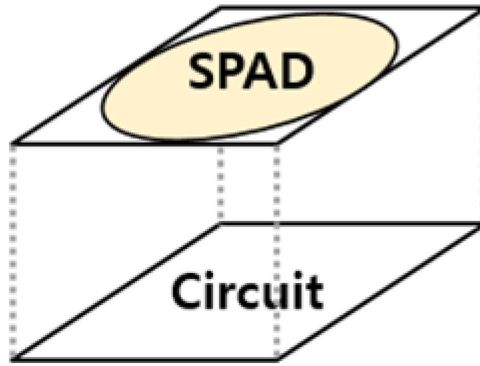

Fig. 1-6. Best configuration of pixel: 3D stacking

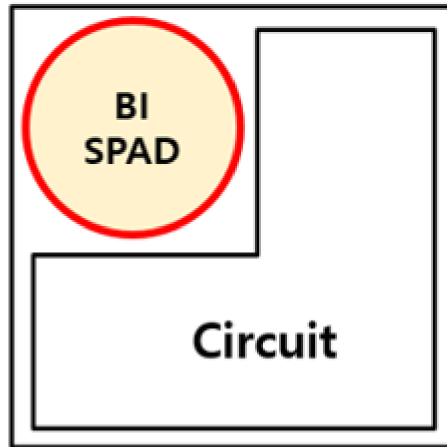

Fig. 1-7. Alternative configuration of pixel

1.6. Outline

This thesis is organized as follows.

- Chapter 2 presents operation of SPAD and AMLED and SPAD's characteristics.
- Chapter 3 presents designed structure of SPAD and compares FI SPAD and BI SPAD.
- Chapter 4 presents the two designed structures of AMLED and experiment results.
- Chapter 5 summarizes the thesis by suggesting the future work.

2. Principle and Characteristics

2.1. Operation of SPAD

As shown in Fig. 2-1, quenching resistor (R_q) is connected in series to the SPAD [21]. Apply a voltage higher than breakdown voltage (V_B) by the excess voltage (V_E) to operate in geiger mode. When the carrier is injected, an electron-hole pair (EHP) is generated because of the photoelectric effect and the current generated by the multiplication of the EHP flows through the R_q. Then the device voltage drops to the V_B. After that, the device voltage is recharged again to the applied voltage (V_B +V_E).

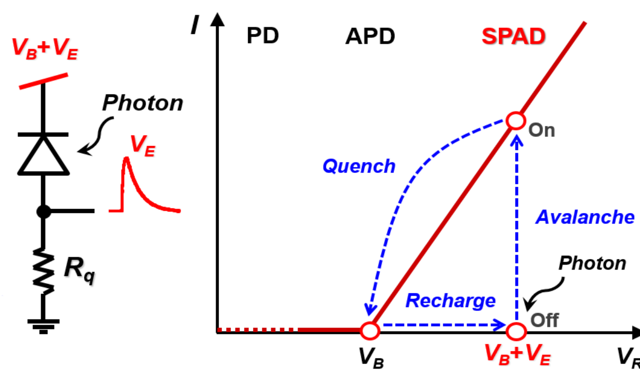

Fig. 2-1. Operation principle of SPAD

2.2. SPAD parameters

In this chapter, look at various factors to check the characteristics of the SPAD. Representatively, there are I-V characteristics, dark count rate (DCR), light emission test (LET), photon detection probability (PDP) and timing jitter as parameters for verifying performance.

2.2.1. I-V Characteristics

A current-voltage experiment is measured to check electrical characteristics such as the breakdown voltage and dark current of the SPAD. In Fig.2-2, the graph when applying reverse voltage to the SPAD is shown. In the dark state, at first it can be seen that a very low current of pA unit flows, but when it exceeds a certain voltage, the current suddenly increases significantly. Normally, the point at which the current greatly increases is considered as breakdown voltage. In the illuminated state, unlike the dark state, it can be seen that a current of several nA flows at breakdown voltage below due to the photo-generated current.

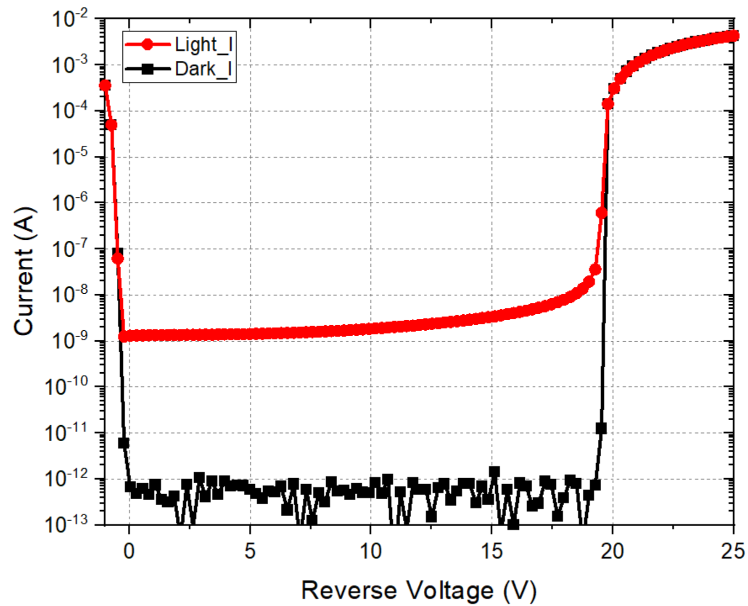

Fig. 2-2. I-V characteristics of a SPAD

2.2.2. DCR

A SPAD operates by generating an avalanche effect with an injected carrier. However, even if there is no injected carrier, an avalanche effect occurs due to the generated carriers. These carriers are called 'Dark carriers' and are represented by the dark count rate (DCR). Since the dark carriers increase mainly by thermal generation, the DCR also tends to increase as the temperature rises [22]. And as the

electric field in the device increases, the dark carriers also increase due to the tunneling noise [23]. Therefore, as the excess voltage increases, and the DCR also increases (Fig. 2-3).

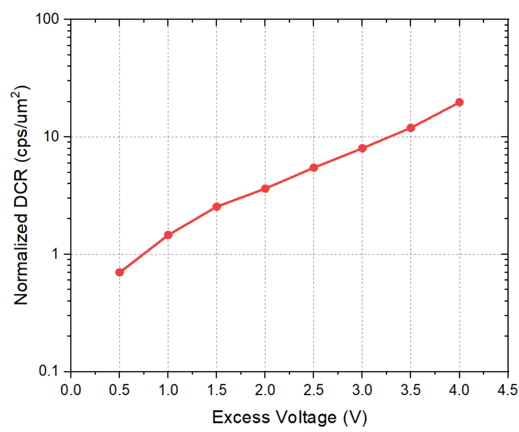

Fig. 2-3. Dark count rate (DCR) of a SPAD

2.2.3. LET

A light emission test (LET) is not exactly a parameter for the SPAD characteristics. Nevertheless, it helps to identify the performance by visually checking the effective active area of the SPAD. When the SPAD is operated in geiger mode, light is emitted

from the device as shown in Fig. 2-4. At this time, if the light is emitted uniformly overall, it works well as a SPAD. However, it can be seen that the efficiency is low if the light is emitted partially or ring shape.

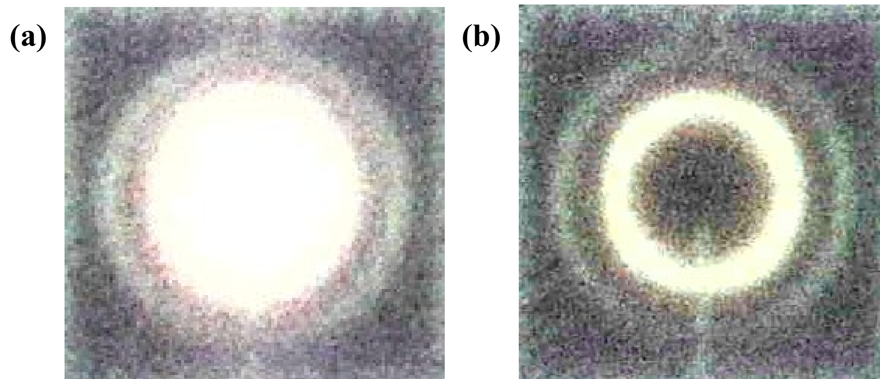

Fig. 2-4. Light emission test (LET) of a SPAD: (a) uniform shape, (b) ring shape

2.2.4. PDP

The photon detection probability (PDP) is one of the most important parameters indicating the efficiency of a SPAD. It is the ratio of photons that generate an avalanche effect among incident photons. As shown in Fig. 2-5, the PDP is proportional to the excess voltage [24]. This is because when the excess voltage

increases, not only the electric field increases but also the depletion region widens, absorbing more photons and being drifted. Another factor that affects the PDP is the wavelength [24]. Depending on the wavelength of the incident light, absorption length and absorption rate are changed, so the PDP is also different. The short wavelength range light is mainly absorbed in the shallow region, and the long wavelength range light is absorbed in the deep region. Therefore, it is necessary to design the structure of the SPAD according to the target.

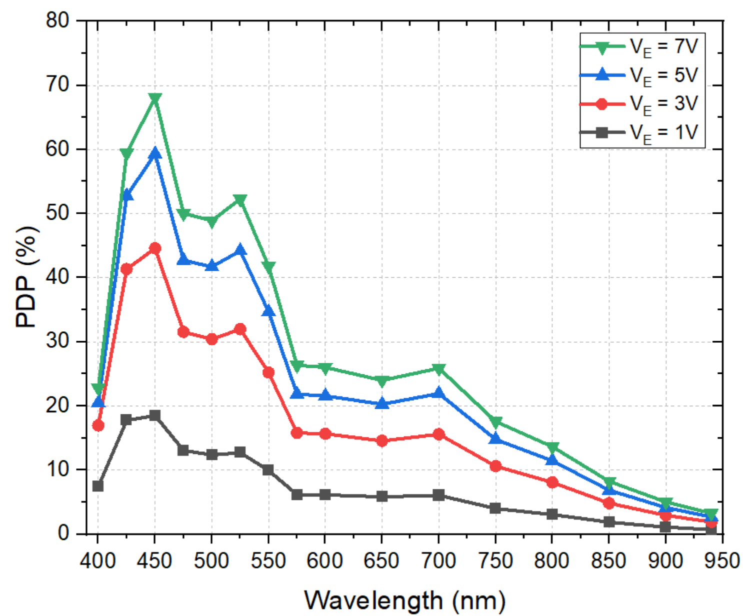

Fig. 2-5. Photon detection probability (PDP) of a SPAD

2.2.5. Timing Jitter

In the SPAD, timing jitter means variation in photon detection time and is defined as full width half maximum (FWHM) [25]. The sample of the timing jitter graph is shown in Fig. 2-6. Timing jitter is a critical parameter because it is related to the performance of depth resolution. For example, if the timing jitter is 1 ns, the depth resolution is 15 cm. Timing jitter depends on excess voltage and wavelength. As the excess voltage increases, the electric field in the depletion region strengthens, so the transit time of the carrier decrease and the variation also decreases. Furthermore, the timing jitter changes because the absorbed range changes according to the wavelength of incident light.

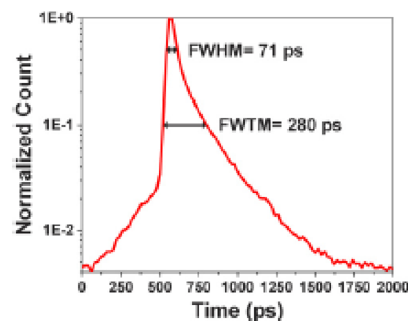

Fig. 2-6. Timing jitter of a SPAD

2.3. Operation of AMLED

A Si LED emits light in the 900nm to 1200nm wavelength range through indirect recombination in forward-mode (FM) (Fig. 2-7(a)). However, when a Si LED is operated in the avalanche breakdown region (avalanche-mode), a high electric field is applied to the Si band and momentum spread occurs through the band-to-band tunneling (Fig. 2-7(b)). As a result, carriers with greater energy emit visible light via recombination (Fig. 2-7(c)) [26], [27].

(a)

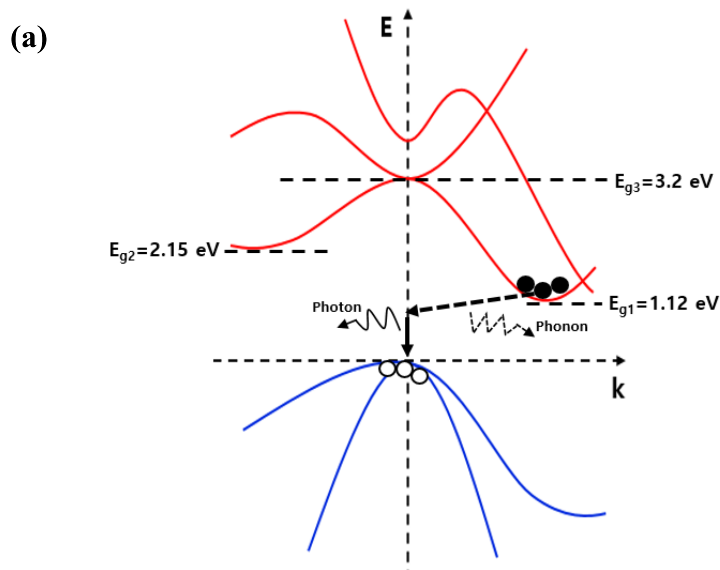

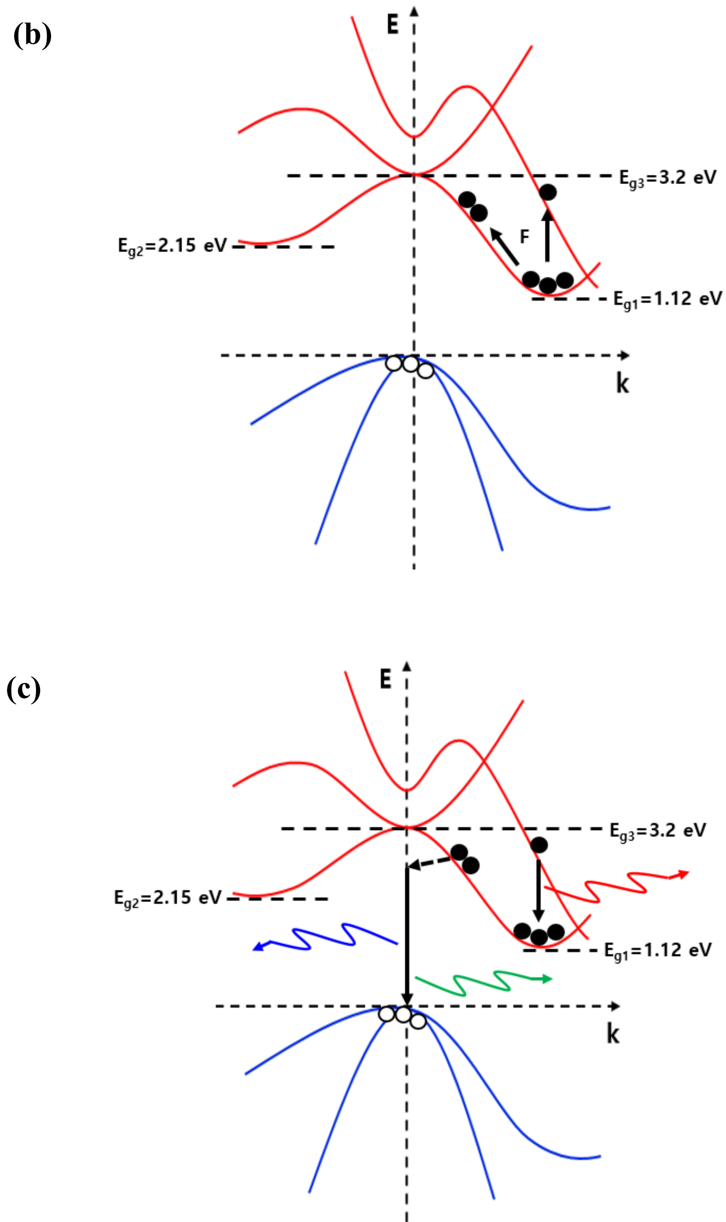

Fig. 2-7. Operation principle of a LED: (a) Forward-mode, (b) Momentum spread of carriers, (c) Avalanche-mode

3. SPAD

3.1. Structures

As shown in Fig. 3-1(a), the existing FI SPAD has multiplication region with P-well/Deep N-well junction. The ‘P+’ acts as an anode and the ‘N+’ acts as a cathode. And the Fig. 3-1(b) is the BI SPAD with the same structure as the FI SPAD, but upside down. However, the substrate of the BI SPAD is thinner than that of the FI SPAD because back-grinding is performed to improve the efficiency. To use the metal under the device as a light reflector, it was made wider than the metal of the FI SPAD.

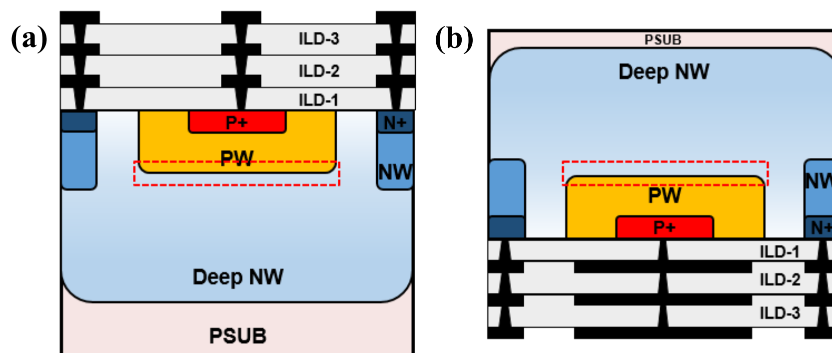

Fig. 3-1. Cross-section of (a) FI SPAD, (b) BI SPAD

3.2. Experiment results

The I-V characteristics are measured in dark states and illuminated states. For setting reverse bias, apply positive voltage to cathode, and set anode and substrate to ground. In the dark state, the dark current and approximate breakdown voltage can be checked. And in the illuminated state, the optical current and more accurate breakdown voltage can be seen. In Fig. 3-2, it is showed the I-V characteristic of BI SPAD. It can be seen that it has a very small dark current in pA units, and it has a breakdown voltage of 16V. In addition, above the breakdown voltage, the current increases rapidly because of the multiplication in the junction.

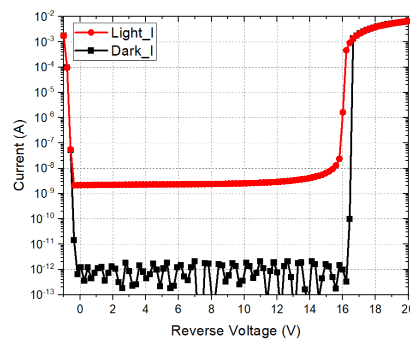

Fig. 3-2. I-V characteristics of the BI SPAD

The DCR is measured from 0.5V to 3V at 0.5V intervals. The value of quenching resistor is 200 kΩ. In theory, the noise characteristics like DCR should be similar, since BI SPAD is just a reverse version of FI SPAD. For effective comparison, normalized DCR is used by dividing the DCR by the area. In Fig. 3-3, the DCR of the BI SPAD is slightly higher than that of the FI SPAD, but this difference can be regarded as a die variation. Even if the BI SPAD actually has a higher DCR, it is not critical because it has a much lower DCR compared to other BI SPADs.

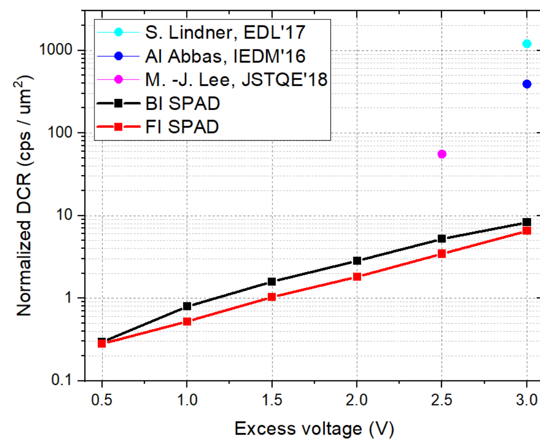

Fig. 3-3. DCR comparison of FI SPAD and BI SPAD

The Fig. 3-4 indicates the relationship between DCR and temperature in FI / BI SPAD. This parameter is important because it can guarantee various environments in applications. Both results show a similar graph and have different tendencies at high and low temperatures. Arrhenius plots from the result of the high temperature results are shown in Fig. 3-5. It was confirmed that the activation energies in FI / BI SPAD are 1.202 eV and 1.197 eV, with little difference. Considering that the bandgap energy of Si is 1.12 eV, it can be seen that noises go directly from the valance band to the conduction band without the effect of defects or traps when they are generated at high temperature. The tendency at low temperature is shown in Fig. 3-6. Since the activation energies are 0.21 eV and 0.19 eV, respectively, it can be confirmed that the trap is affected during the noise generation process. However, because the DCR is very low at the low temperature, it is not critical for applications.

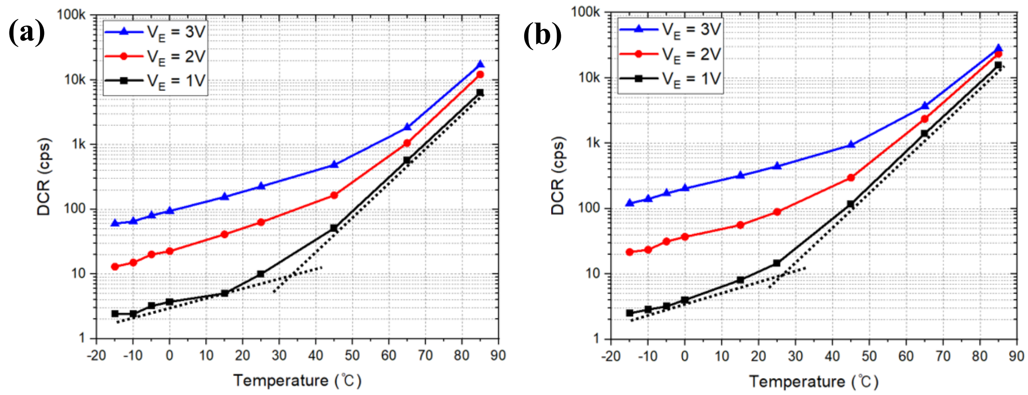

Fig. 3-4. The relationship between DCR and temperature: (a) FI SPAD, (b) BI SPAD

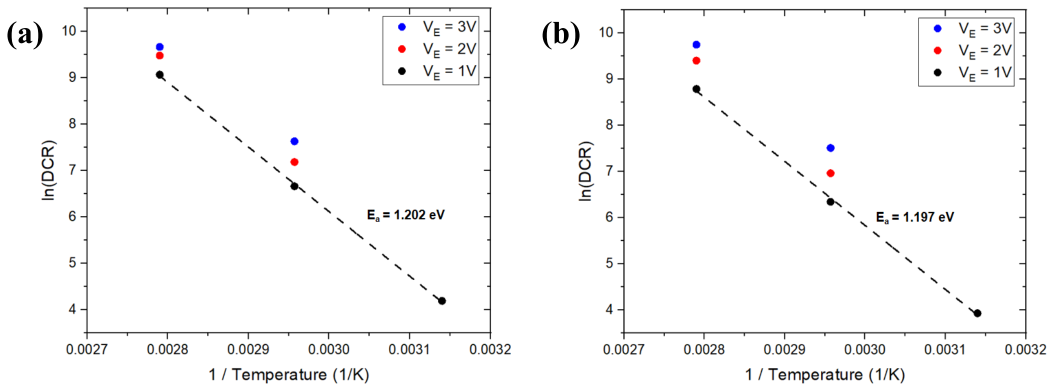

Fig. 3-5. The Arrhenius plot at high temperature: (a) FI SPAD, (b) BI SPAD

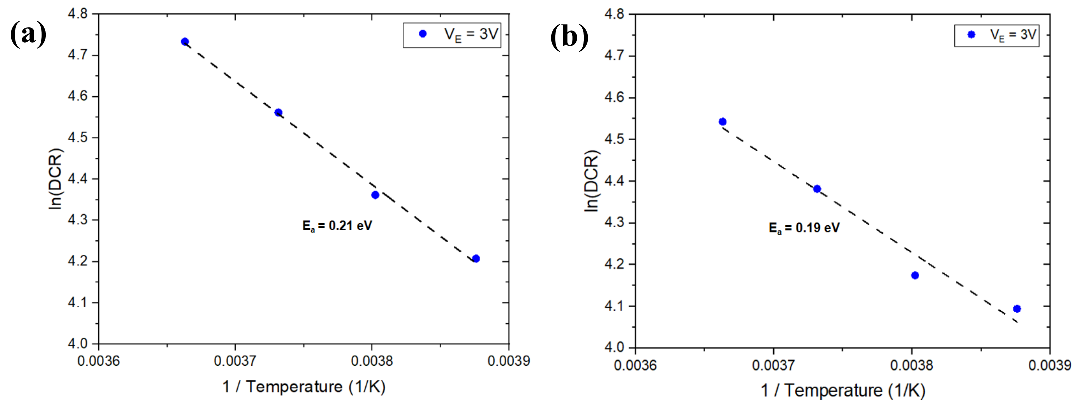

Fig. 3-6. The Arrhenius plot at low temperature: (a) FI SPAD, (b) BI SPAD

The LET is measured over 3V above breakdown voltage. Fig. 3-7 shows the BI SPAD also emitted uniform light across the overall active area like the FI SPAD. Looking at the two LET results, it can be seen that BI SPAD emits red light and FI SPAD emits white light. This is due to the depth of the junction. The junction depth of FI SPAD is shallow, light emitted from the junction passes through Si almost intact. However, the junction depth is deep for BI SPAD so the short wavelength light like blue ray is absorbed as it passes through Si. Therefore, emitted light from BI SPAD has a relatively red color.

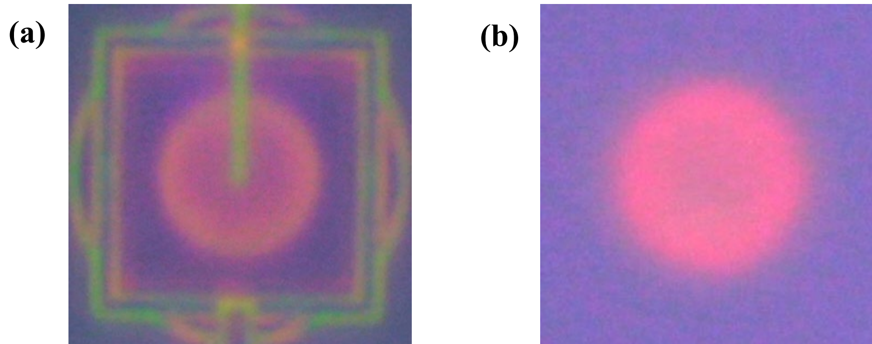

Fig. 3-7. LET results under the same illuminated conditions: (a) FI SPAD at V_E = 3V, (b) BI SPAD at V_E = 3V

The PDP value was measured up to V_E=3V since it is saturated from 4V. As shown in Fig. 3-8, when the excess bias voltage is 3V, the peak PDP of the BI SPAD is about 50% at 600 nm and PDP is 10% at 940 nm. The 940 nm is important for ranging applications because 940 nm is the eye-safety wavelength range. And although it is general that it continues to decrease after the first peak, PDP seems to rise again around 700 nm due to the metal reflector. In Fig. 3-9, the peak PDP of the FI SPAD is 60% at 500 nm and PDP at 940 nm is 3%. Comparing the BI SPAD and FI SPAD, although FI SPAD has higher peak PDP, BI SPAD has higher PDP

from 600 nm. And most importantly, the PDP of the BI SPAD at 940 nm increased more than three times compared to the FI SPAD.

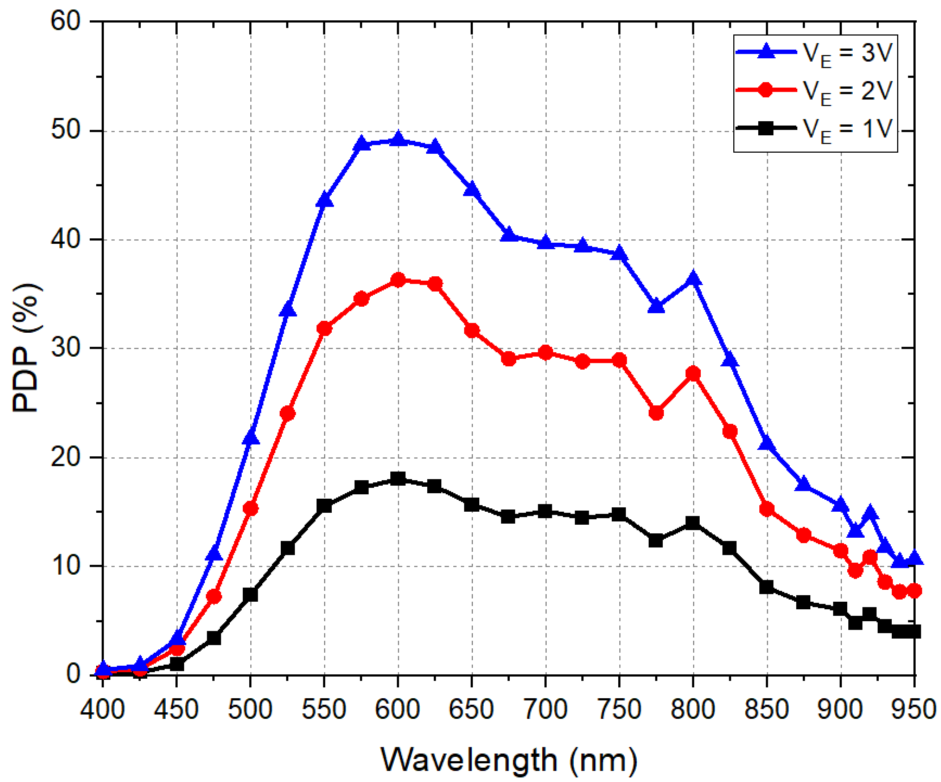

Fig. 3-8. PDP of the BI SPAD at V_E = 1V, 2V, 3V

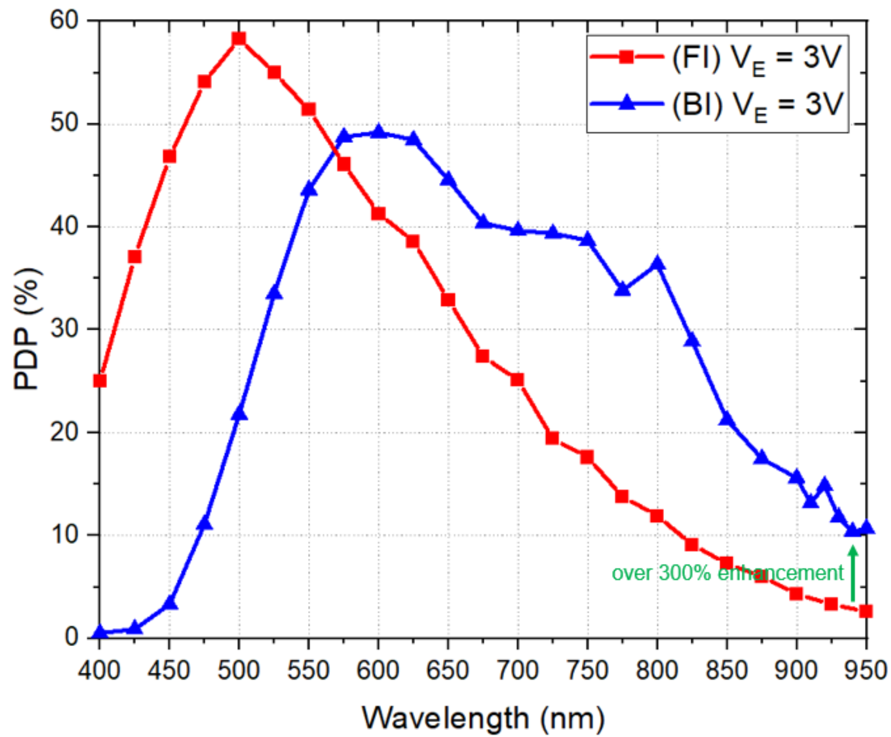

Fig. 3-9. PDP comparison between FI SPAD and BI SPAD at $V_E = 3V$

Let's analyze this quantitatively through process information and TCAD simulation. The Fig. 3-10 follows the process information. The red dotted line indicates the main junction. The thickness of Si is 3.3 um, the depth of deep NW is 3 um, and the depth of the junction from the surface is 2.2 um.

According to the Fig. 3-11, the absorption length of 400~450 nm wavelength light is 0.1~0.3 um. Therefore, it has a low PDP because it does not reach the junction and is absorbed by the substrate. The absorption length of 575~625 nm light is 2~3 um. It has a high PDP in this wavelength range because it is consistent with the junction depth. Finally, the absorption depth of light with a wavelength range of 650~750 nm is 3.5~6 um. Considering that the thickness of Si is 3.3 um, it can be seen that the metal reflector worked as intended, and accordingly, PDP increased in this wavelength range.

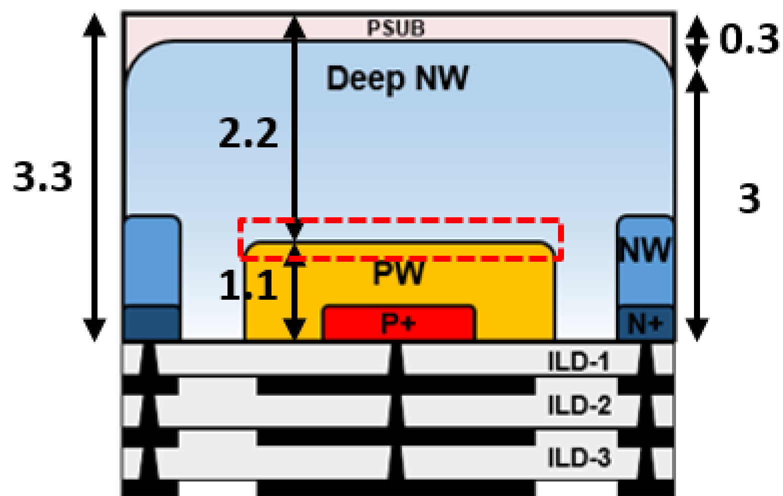

Fig. 3-10. Depth information of the BI SPAD

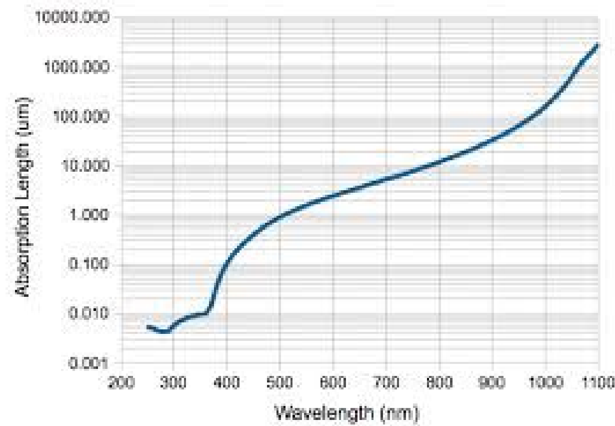

Fig. 3-11. Absorption length according to the wavelength in Si

The TCAD simulation is a tool that assists in the designed devices, light absorption can be checked in advance [28-30]. In Synopsys Sentaurus TCAD, the structure is designed using the given doping profile and the Sentaurus Structure Editor (SDE). The illuminated condition is confirmed using the SDevice. Absorption criteria followed the definition of absorption length. The Fig. 3-12 is the TCAD result showing the doping concentration. In fact, it was confirmed that the junction was formed at a depth of about 2 μm from the surface. In Fig. 3-13, most of the 400-450 nm light is absorbed near the surface. The red line means junction depth. It is confirmed that light of 575~625 nm not only hits the junction, but some is reflected

by the metal reflector. And a large part of 650~750 nm light is reflected by the metal reflector. As a result, it appears that the TCAD simulation results are consistent with the actual PDP results.

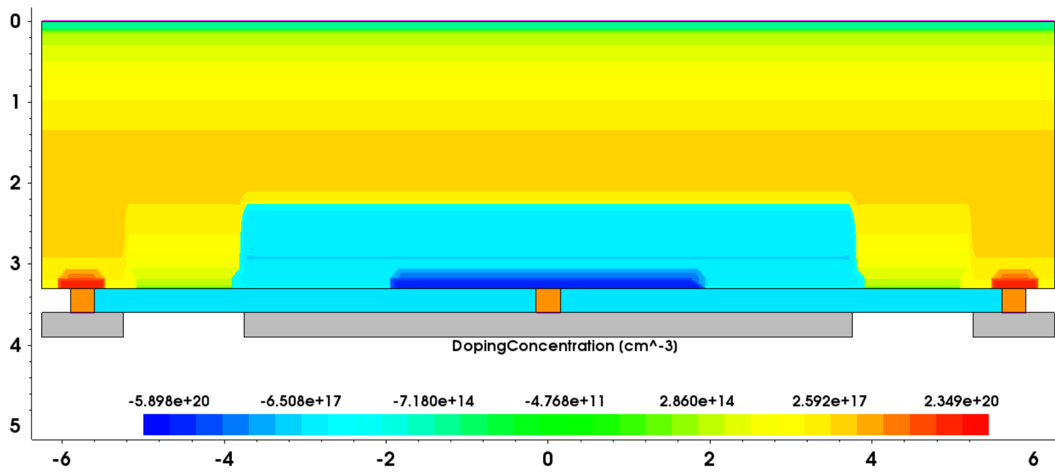

Fig. 3-12. Doping profile of the BI SPAD with TCAD simulation

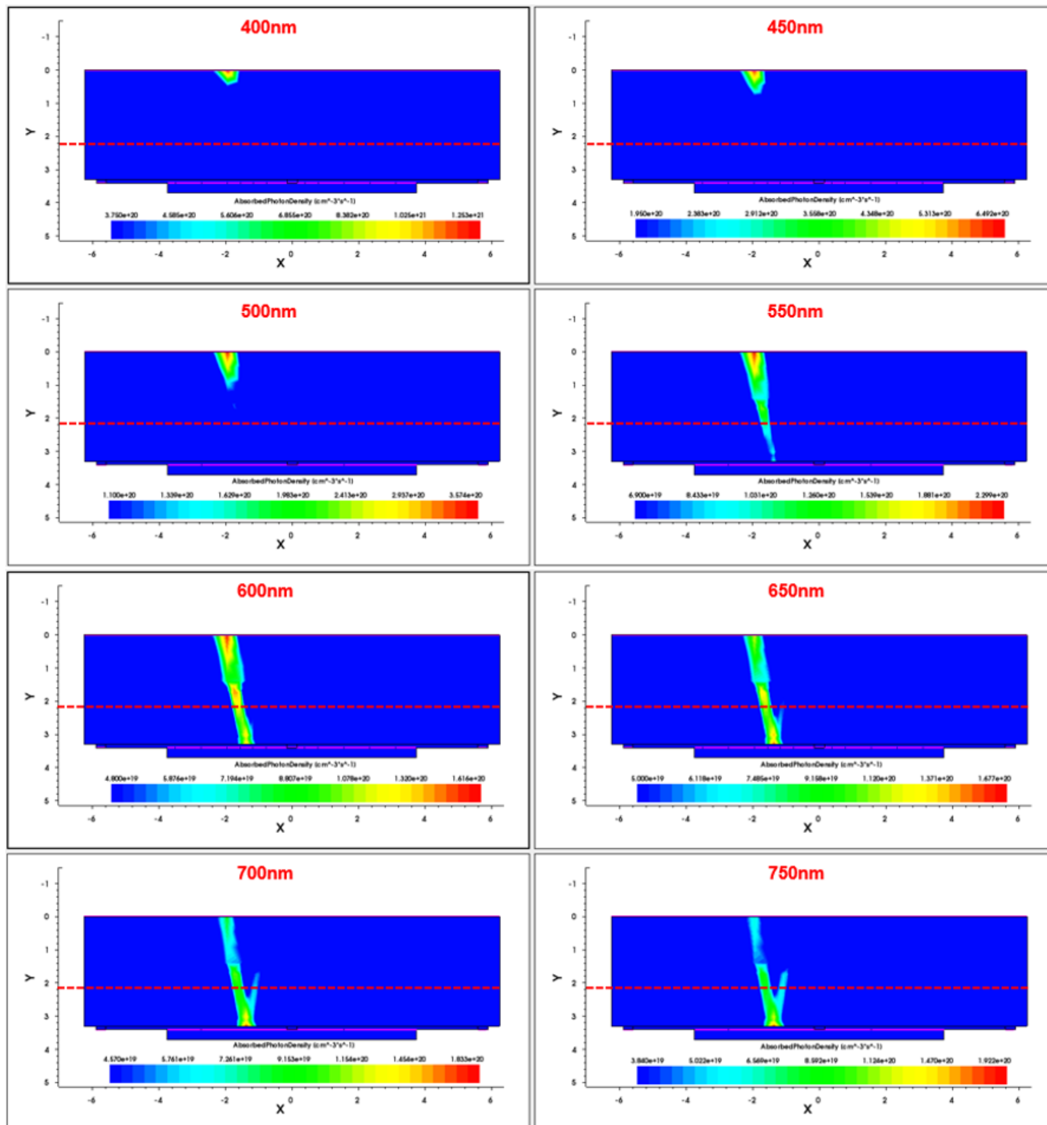

Fig. 3-13. Reflection by metal reflector depending on the wavelength with TCAD simulation

The Timing Jitter is measured using the time-correlated single-photon counting (TCSPC) method with a 940 nm pulsed laser. And the value includes the jitter of the laser and laser driver. In Fig. 3-14, the timing jitter at 940 nm of the FI SPAD is 71 ps full width half maximum (FWHM) when Vex=3V. And the timing jitter at 940 nm of the BI SPAD is 72 ps FWHM when Vex=3V. The timing jitter value was confirmed to be similar to FI SPAD and BI SPAD. The reason seems to be that the designed SPAD is a PN type. Since a reverse bias is applied between the deep NW and the substrate, carriers absorbed by the substrate cannot reach the junction. That is, both FI SPAD and BI SPAD have similar actual absorption ranges. Therefore, the timing jitter value is also similar. However, the diffusion tail of BI SPAD is longer than that of FI SPAD. This seems to be the effect of the metal reflector. Since the reflected incident light is absorbed again, the effective diffusion length increases than that of FI SPAD. Therefore, the diffusion tail of BI SPAD is longer.

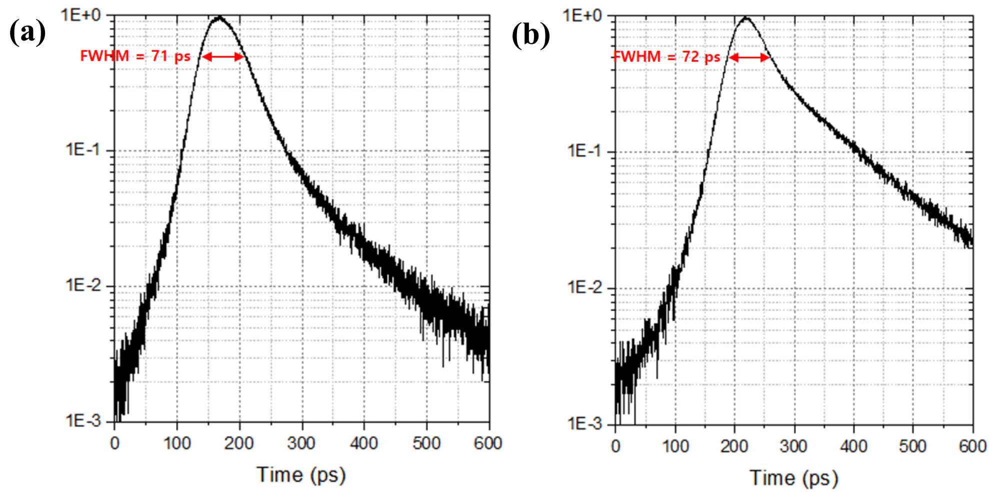

Fig. 3-14. Timing jitter results at 940 nm: (a) FI SPAD, (b) BI SPAD

Table 1 provides an overall summary and performance comparison, which is recently reported BI SPAD based CMOS technology. The BI SPAD reported in this work shows the higher PDP at 940 nm than others reported in [31], [32] and [33]. It also has higher peak PDP and better noise characteristics compared to other BI SPADs. The BI SPAD reported in [34] has higher PDP at 940nm, but the device information is insufficient, and in-house technology is used instead of standard CMOS technology.

	FI SPAD	BI SPAD	[31]	[32]	[33]	[34]
Technology	110 nm CIS (FI)	110 nm CIS (BI)	65 nm CIS (BI)	65 nm CIS (BI)	45 nm CIS (BI)	90 nm (BI)
Junction	PW/DNW	PW/DNW	PW/DNW	PW/DNW	P+DNW	n.a.
Guard Ring	Virtual GR	Virtual GR	Virtual GR	Virtual GR	Physical GR	n.a.
V_B	14V	16V	12V	n.a.	28.5V	22V
V_E	3V	3V	3V	4.4V	2.5V	3V
Normalized DCR	6.5 cps/μm^2	8.3 cps/μm^2	391.4 cps/μm^2	2,463.1 cps/μm^2	55.4 cps/μm^2	19 cps/pix
PDP Peak	58.3% @ 500 nm	58.9% @ 600 nm	27.5% @ 640 nm	29.5% @ 660 nm	31.8% @ 600 nm	66.7% @ 650 nm
PDP @ 940 nm	3%	10.4%	7%	5.5%	4%	20.2% (PDE)

Table 1. Summary and comparison of the state-of-the-art BI SPADs

4. AMLED

4.1. structure

In Fig. 4-1(a), the SPAD has P-well/Deep N-well junction called 'deep structure'. And it has virtual guard ring. And in Fig 4-1(b), the SPAD has P+/N-well junction called 'shallow structure', because it has relatively shallow junction than the previous structure. In this structure, P-well region (guard ring) is used to prevent edge breakdown. In addition, considering the application as a LED, it was manufactured in the array form.

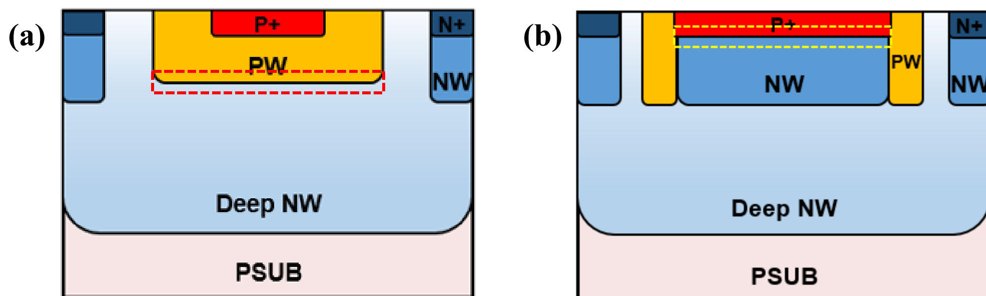

Fig. 4-1. Structures of AMLED: (a) Deep structure, (b) Shallow structure

4.2. Experiment Results

In this thesis, light emission test (LET) and electroluminescence (EL) were proceeded to measure the performance of the AMLEDs. LET was performed under the same illuminated conditions. In Fig. 4-2 and Fig. 4-3, the LET results of deep structure and shallow structure are different. The result of the deep structure is relatively reddish than that of the shallow structure. This is related to the junction depth. Because the junction depth of the deep structure is deeper than that of the shallow structure, blue light emitted from the junction is absorbed in the process of coming out to the surface. Therefore, it has a relatively red color. This can also be confirmed by the EL results. In Fig. 4-4, it can be seen that the EL result of the shallow structure is shifted toward a shorter wavelength than that of the deep structure. That is, it was confirmed that the shallow structure emits more blue light to the surface, giving a relatively white color.

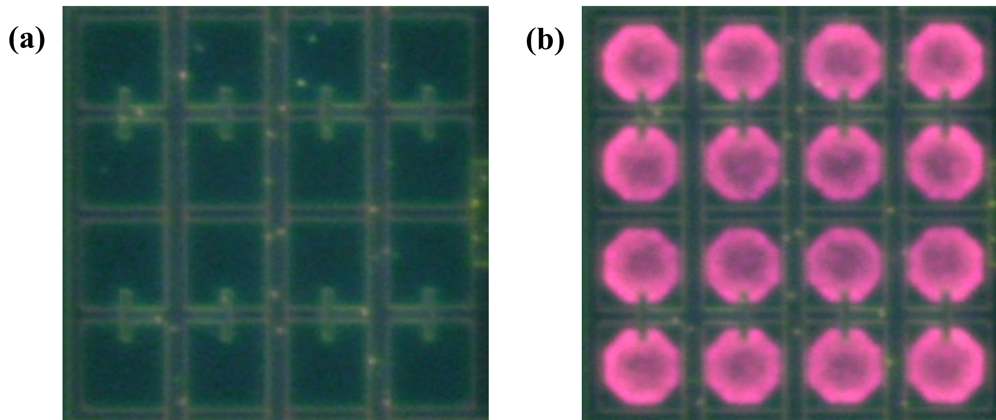

Fig. 4-2. LET results of deep junction structure: (a) before the breakdown voltage, (b) after the breakdown voltage (V_E = 3V)

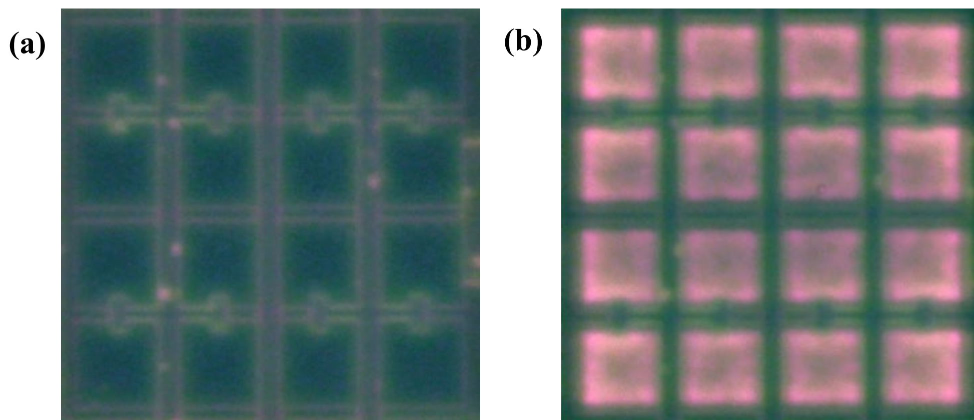

Fig. 4-3. LET results of shallow junction structure: (a) before the breakdown voltage, (b) after the breakdown voltage (V_E = 3V)

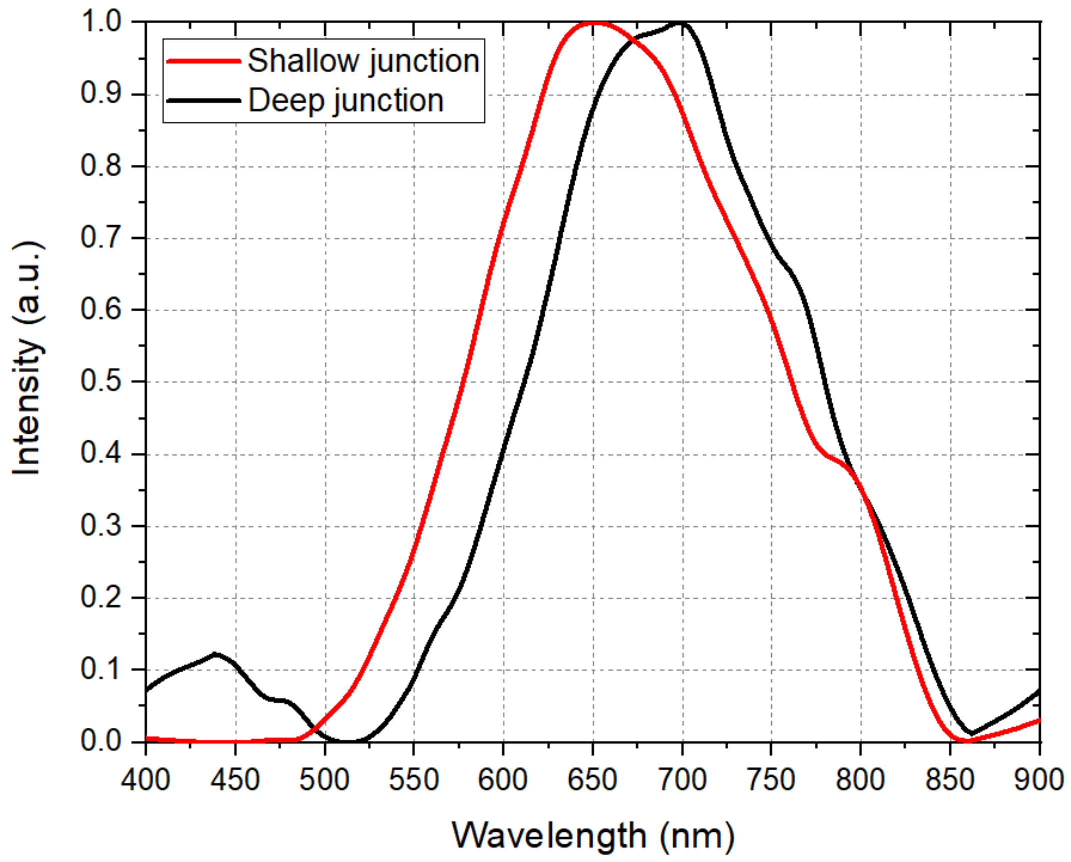

Fig. 4-4. EL result of deep junction and shallow junction

5. Conclusion

In general, front-illuminated SPADs (FI SPADs) are mainly used in ranging applications due to the ease of manufacture. However, it has limitations in that long-wavelength detection efficiency is low and injection loss is caused by metal and dielectric layers over the device.

In this thesis, I proposed a back-illuminated SPAD (BI SPAD), which reversed the FI SPAD and compared in various characteristics. The DCR value increased slightly compared to the FI SPAD, but it was still very low compared to other BI SPADs. And the LET result was still uniform. Through this, it was confirmed that the device was not damaged during the back-etching process for a BI SPAD. The PDP value at 940 nm, which we target, increased more than three times compared to the FI SPAD. This is attributed to the deeper junction depth from the surface. In addition, the detection efficiency in the overall long-wavelengths was also improved because the incident light was reflected by the metal reflector and absorbed again. This effect was demonstrated through the TCAD simulation. Also, the timing jitter,

which is a depth resolution parameter, was almost the same as that of the FI SPAD. Because carriers absorbed in the p-substrate cannot participate in drift mechanism. However, the diffusion tail of the BI PSAD was increased compared to the FI SPAD as the effective diffusion length was increased due to the metal reflector. As a result, efficiency in the near-infrared (NIR) wavelength range is improved without significant deterioration in other parameter. It is expected that the BI SPAD is able to play an important role in the emerging applications requiring higher NIR efficiency.

In addition, the applicability of the SPAD as an LED was confirmed. Normally, since Si LED emits the short wave infrared (SWIR) light, it could not replace III-V LEDs. But it was shown that visible light is emitted when operated in the avalanche range. I designed two array structures with different junction depths and checked the wavelength selectivity. In fact, the LET result of the shallow structure looks whiter than that of the deep structure because emitted light from shallow junction include more blue light. It is also proved by the EL results. Through these results, it is expected that AMLEDs will be able to substitute III-V LEDs.

Reference

[1] S. Cova, M. Ghioni, A. Lacaita, C. Samori, and F. Zappa, "Avalanche photodiodes and quenching circuits for single-photon detection," Appl. Opt. 35, 1956-1976 (1996).

[2] D. Stoppa, L. Pancheri, M. Scandiuzzo, L. Gonzo, G. -F. Dalla Betta and A. Simoni, "A CMOS 3-D Imager Based on Single Photon Avalanche Diode," in IEEE Transactions on Circuits and Systems I: Regular Papers, vol. 54, no. 1, pp. 4-12, Jan. 2007.

[3] C. Niclass, M. Gersbach, R. Henderson, L. Grant and E. Charbon, "A Single Photon Avalanche Diode Implemented in 130-nm CMOS Technology," in IEEE Journal of Selected Topics in Quantum Electronics, vol. 13, no. 4, pp. 863-869, July-aug. 2007.

[4] J. -M. Lee, S. -H. Cho and W. -Y. Choi, "An Equivalent Circuit Model for a Ge Waveguide Photodetector on Si," in IEEE Photonics Technology Letters, vol. 28, no. 21, pp. 2435-2438, 1 Nov.1, 2016.

[5] Y. Kang *et al.*, “Monolithic germanium/silicon avalanche photodiodes with 340GHz gain-bandwidth product,” *Nature Photonics*, vol. 3, no. 1, pp. 59–63, 2009.

[6] S. Cova, A. Longoni, and A. Andreoni, “Towards picosecond resolution with single-photon avalanche diodes,” *Review of Scientific Instruments*, vol. 52, no. 3, pp. 408–412, 1981.

[7] A. Rochas, A. R. Pauchard, P. A. Besse, D. Pantic, Z. Prijic and R. S. Popovic, "Low-noise silicon avalanche photodiodes fabricated in conventional CMOS technologies," in IEEE Transactions on Electron Devices, vol. 49, no. 3, pp. 387-394, March 2002.

[8] M. -J. Lee and W. -Y. Choi, "Area-Dependent Photodetection Frequency Response Characterization of Silicon Avalanche Photodetectors Fabricated With Standard CMOS Technology," in IEEE Transactions on Electron Devices, vol. 60, no. 3, pp. 998-1004, March 2013.

[9] I. Vornicu, F. Bandi, R. Carmona-Galán and Á. Rodríguez-Vázquez, "Low-Noise and High-Efficiency Near-IR SPADs in 110nm CIS Technology," ESSDERC 2019 - 49th European Solid-State Device Research Conference (ESSDERC), 2019, pp. 250-253.

[10] M. Gersbach, C. Niclass, E. Charbon, J. Richardson, R. Henderson and L. Grant, "A single photon detector implemented in a 130nm CMOS imaging process," ESSDERC 2008 - 38th European Solid-State Device Research Conference, 2008, pp. 270-273.

[11] Won-Yong Ha, Eunsung Park, Byungchoul Park, Youngcheol Chae, Woo-Young Choi, and Myung-Jae Lee, "Noise optimization of single-photon avalanche diodes fabricated in 110 nm CMOS image sensor technology," Opt. Express 30, 14958-14965 (2022).

[12] M. -J. Lee et al., "High-Performance Back-Illuminated Three-Dimensional Stacked Single-Photon Avalanche Diode Implemented in 45-nm CMOS Technology," in IEEE Journal of Selected Topics in Quantum Electronics, vol. 24, no. 6, pp. 1-9, Nov.-Dec. 2018.

[13] Green, M., Zhao, J., Wang, A. et al., “Efficient silicon light-emitting diodes,” in Nature 412, 805–808 (2001).

[14] Thorsten Trupke, Jianhua Zhao, Aihua Wang, Richard Corkish, and Martin A. Green, "Very efficient light emission from bulk crystalline silicon", Appl. Phys. Lett. 82, 2996-2998 (2003).

[15] A. G. Chynoweth and K. G. McKay, “Photon emission from Avalanche Breakdown in Silicon,” Phys. Rev. 102(2), 369–376 (1956).

[16] M. du Plessis, H. Aharoni and L. W. Snyman, "Silicon LEDs fabricated in standard VLSI technology as components for all silicon monolithic integrated optoelectronic systems," in IEEE Journal of Selected Topics in Quantum Electronics, vol. 8, no. 6, pp. 1412-1419, Nov.-Dec. 2002.

[17] L.W. Snyman, M. du Plessis, and H. Aharoni, “Injection-Avalanche-Based n+ pn Silicon Complementary Metal Oxide Semiconductor Light-Emitting Device (450 - 750 nm) with 2-Order-of-Magnitude Increase in Light Emission Intensity,” Jpn. J. Appl. Phys. 46(4B), 2474–2480 (2007).

[18] Satadal Dutta, Raymond J. E. Hueting, Anne-Johan Annema, Lin Qi, Lis K. Nanver, and Jurriaan Schmitz , "Opto-electronic modeling of light emission from

avalanche-mode silicon p^+n junctions", Journal of Applied Physics 118, 114506 (2015).

[19] E. Charbon, M. Scandini, J. Mata Pavia and M. Wolf, "A dual backside-illuminated 800-cell multi-channel digital SiPM with 100 TDCs in 130nm 3D IC technology," 2014 IEEE Nuclear Science Symposium and Medical Imaging Conference (NSS/MIC), 2014, pp. 1-4.

[20] J. M. Pavia, M. Scandini, S. Lindner, M. Wolf and E. Charbon, "A 1 × 400 Backside-Illuminated SPAD Sensor With 49.7 ps Resolution, 30 pJ/Sample TDCs Fabricated in 3D CMOS Technology for Near-Infrared Optical Tomography," in IEEE Journal of Solid-State Circuits, vol. 50, no. 10, pp. 2406-2418, Oct. 2015.

[21] Chockalingam Veerappan, "Single-photon avalanche diodes for cancer diagnosis," Ph.D. dissertation, TU Delft, Delft University of Technology, 2016.

[22] A. J. P. T. Peter Seitz, "Single-photon imaging," Springer, 1995.

[23] M. A. Itzler, r. Ben-Michael, C. -F. Hsu, K. Slomkowski, A. Tosi, S. Cova, F. Zappa & R. Ispasoiu (2007) Single photon avalanche diodes (SPADs) for 1.5 μm photon counting applications, Journal of Modern Optics, 54:2-3, 283-304.

[24] S. Cova, M. Ghioni, M. A. Itzler, J. C. Bienfang, and A. Restelli, "Semiconductor-based detectors", Elsevier, 2013.

[25] Myung-Jae Lee, Pengfei Sun, and Edoardo Charbon, "A first single-photon avalanche diode fabricated in standard SOI CMOS technology with a full characterization of the device," Opt. Express 23, 13200-13209 (2015).

[26] L. W. Snyman, M. du Plessis and E. Bellotti, "Photonic Transitions (1.4 eV–2.8 eV) in Silicon p^+np^+ injection-avalanche CMOS LEDs as Function of Depletion Layer Profiling and Defect Engineering," in IEEE Journal of Quantum Electronics, vol. 46, no. 6, pp. 906-919, June 2010.

[27] M. Lahbabi,A. Ahaitouf,M. Fliyou,E. Abarkan,J.-P. Charles, A. Bath, A. Hoffmann, S.E. Kerns and D.V. Kerns, Jr., "Analysis of electroluminescence spectra of silicon and gallium arsenide p-n junctions in avalanche breakdown," J. Appl. Phys., vol. 95, no.4, pp. 1822-1828, 2004.

[28] M. -J. Lee and W. -Y. Choi, "Performance Optimization and Improvement of Silicon Avalanche Photodetectors in Standard CMOS Technology," in IEEE Journal of Selected Topics in Quantum Electronics, vol. 24, no. 2, pp. 1-13, March-April 2018.

[29] K. Xu et al., "Design and Fabrication of a Monolithic Optoelectronic Integrated Si CMOS LED Based on Hot-Carrier Effect," in IEEE Journal of Selected Topics in Quantum Electronics, vol. 22, no. 6, pp. 70-77, Nov.-Dec. 2016.

[30] K. Xu, “Monolithically integrated Si gate-controlled light-emitting device: science and properties,” J. Opt., vol. 20, no. 2, Jan. 2018.

[31] T. Al Abbas, N. A. W. Dutton, O. Almer, S. Pellegrini, Y. Henrion and R. K. Henderson, "Backside illuminated SPAD image sensor with 7.83µm pitch in 3D-stacked CMOS technology," 2016 IEEE International Electron Devices Meeting (IEDM), 2016.

[32] S. Lindner, S. Pellegrini, Y. Henrion, B. Rae, M. Wolf and E. Charbon, "A High-PDE, Backside-Illuminated SPAD in 65/40-nm 3D IC CMOS Pixel With Cascoded Passive Quenching and Active Recharge," in IEEE Electron Device Letters, vol. 38, no. 11, pp. 1547-1550, Nov. 2017.

[33] M. -J. Lee et al., "High-Performance Back-Illuminated Three-Dimensional Stacked Single-Photon Avalanche Diode Implemented in 45-nm CMOS Technology," in IEEE Journal of Selected Topics in Quantum Electronics, vol. 24, no. 6, pp. 1-9, Nov.-Dec. 2018.

[34] S. Shimada et al., "A Back Illuminated 6 µm SPAD Pixel Array with High PDE and Timing Jitter Performance," 2021 IEEE International Electron Devices Meeting (IEDM), 2021, pp. 20.1.1-20.1.4.

Abstract in Korean

CMOS 기술로 제작된 후면조사 Single-Photon Avalanche Diodes 와 Avalanche-Mode Light Emitting Diodes

연세대학교 대학원

전기전자공학과

엄 도 윤

Complementary metal-oxide-semiconductor (CMOS) 공정에서 제작된 single-photon avalanche diode (SPAD)는 이미징 및 거리 측정, 양자 통신 및

네트워크, 생물학, 화학, 천문학 등과 같은 여러 응용 분야에서 사용되고 있다. 그 중에서 특히, 자율주행자동차 및 3D 스캐너를 위한 LiDAR 응용으로 각광받고 있다. 기존에는 전면조사 SPAD 가 사용되고 있었으나, 빛이 흡수되는 영역이 얕아 장파장에서의 낮은 효율을 갖는다는 한계를 가지고 있다. 따라서 본 논문에서는 기존의 소자를 뒤집어서 장파장 효율을 최적화시킨 형태의 후면조사 SPAD 구조를 제시한다. 본 논문에서 제시한 SPAD 는 P-well/Deep N-well 구조를 가지고, DB Hitek 의 110 nm BI CIS 공정을 이용하여 제작되었다. 측정 결과 noise 특성의 큰 변화없이, 제시된 후면조사 SPAD 가 기존의 전면조사 SPAD 보다 3 배 이상 높은 940 nm PDP 값을 갖는 것을 확인하였다.

다음으로 본 논문에서는 CMOS 공정을 이용하여 제작한 array 형태의 Si LED 를 avalanche 영역에서 작동시킴으로써, 가시광선 영역에서의 동작 특성을 확인하였다. 또한 접합의 깊이가 서로 다른 두 가지

구조의 LET 및 EL 측정을 통해 실제 LED 로서 응용 가능성을 확인하였다.

Keywords: 단일광자검출소자, 거리측정센서, 광소자, 포토다이오드, 표준 CMOS 공정, 전면조사, 후면조사, 발광다이오드, avalanche-mode